Nuclear Magnetic Resonance Spectroscopy on a (5-Nanometer)^3 Sample Volume

T. Staudacher *et al.*

Science **339**, 561 (2013);
DOI: 10.1126/science.1231675

Nuclear Magnetic Resonance Spectroscopy on a (5-Nanometer)^3 Sample Volume

T. Staudacher,[1,2] F. Shi,[3] S. Pezzagna,[4] J. Meijer,[4] J. Du,[3] C. A. Meriles,[5] F. Reinhard,[1]* J. Wrachtrup[1]

Application of nuclear magnetic resonance (NMR) spectroscopy to nanoscale samples has remained an elusive goal, achieved only with great experimental effort at subkelvin temperatures. We demonstrated detection of NMR signals from a (5-nanometer)^3 voxel of various fluid and solid organic samples under ambient conditions. We used an atomic-size magnetic field sensor, a single nitrogen-vacancy defect center, embedded ~7 nanometers under the surface of a bulk diamond to record NMR spectra of various samples placed on the diamond surface. Its detection volume consisted of only 10^4 nuclear spins with a net magnetization of only 10^2 statistically polarized spins.

Nuclear magnetic resonance (NMR) spectroscopy (*1*, *2*) provides a label-free method for chemical analysis, provided that there is sufficient sample for detection. Much effort has been directed to applying NMR to nanoscale samples. Indeed, NMR detection of a (4 nm)^3 voxel of protons has been achieved with magnetic resonance force microscopy, a challenging experimental technique operating at ultralow temperature in vacuum (*3*, *4*). Under ambient conditions, microcoil detectors have enabled the detection of liquid samples of (3000 nm)^3 volume, but further miniaturization of this technique is not straightforward (*5*, *6*).

Recently, single nitrogen-vacancy (NV) centers in diamond (*7*, *8*) have been proposed as a novel atomic-size magnetic field sensor for detecting nanoscale nuclear spin ensembles or even single nuclear spins (*9*). This center is a joint defect in the carbon lattice of diamond, consisting of a substitutional nitrogen atom and an adjacent vacancy. Its spin triplet (spin 1) ground state can be polarized and read out optically, so that electron spin resonance experiments can be performed on a single spin. A single center can be used as a nanoscale magnetic field sensor, able to detect a magnetic field in the nanotesla range in an integration time of 1 s (*10*). This corresponds to the field of a single nuclear spin at a distance of a few nanometers (*9*). Indeed, detection of single ^{13}C nuclear spins has recently been reported, located inside the diamond lattice a few nanometers from the NV center (*11*–*13*).

Here we demonstrate detection of proton (^{1}H) nuclear spins in various liquid and solid samples placed on the diamond surface. This is a key milestone toward achieving nanoscale magnetic resonance imaging based on scanning NV centers (*14*, *15*). The technique additionally allows one to perform NMR on an arbitrary sample in the regime of ultralow and zero magnetic field, because it is based on statistical rather than thermal polarization of the nuclei. Further, our results are an inital step toward efficient hyperpolarization of any organic sample by the coherent transfer of polarization from the optically and fully polarized NV center.

We used the experimental setup sketched in Fig. 1A. Single NV centers were created 2.5 to

[1]3rd Physics Institute and Research Center SCoPE, University of Stuttgart, 70569 Stuttgart, Germany. [2]Max Planck Institute for Solid State Research, 70174 Stuttgart, Germany. [3]Hefei National Laboratory for Physics Sciences at Microscale and Department of Modern Physics, University of Science and Technology of China, Hefei, 230026, China. [4]RUBION, Ruhr-Universität Bochum, 44801 Bochum, Germany. [5]Department of Physics, The City College of New York, CUNY New York, NY 10031, USA.

*To whom correspondence should be addressed. E-mail: f.reinhard@physik.uni-stuttgart.de

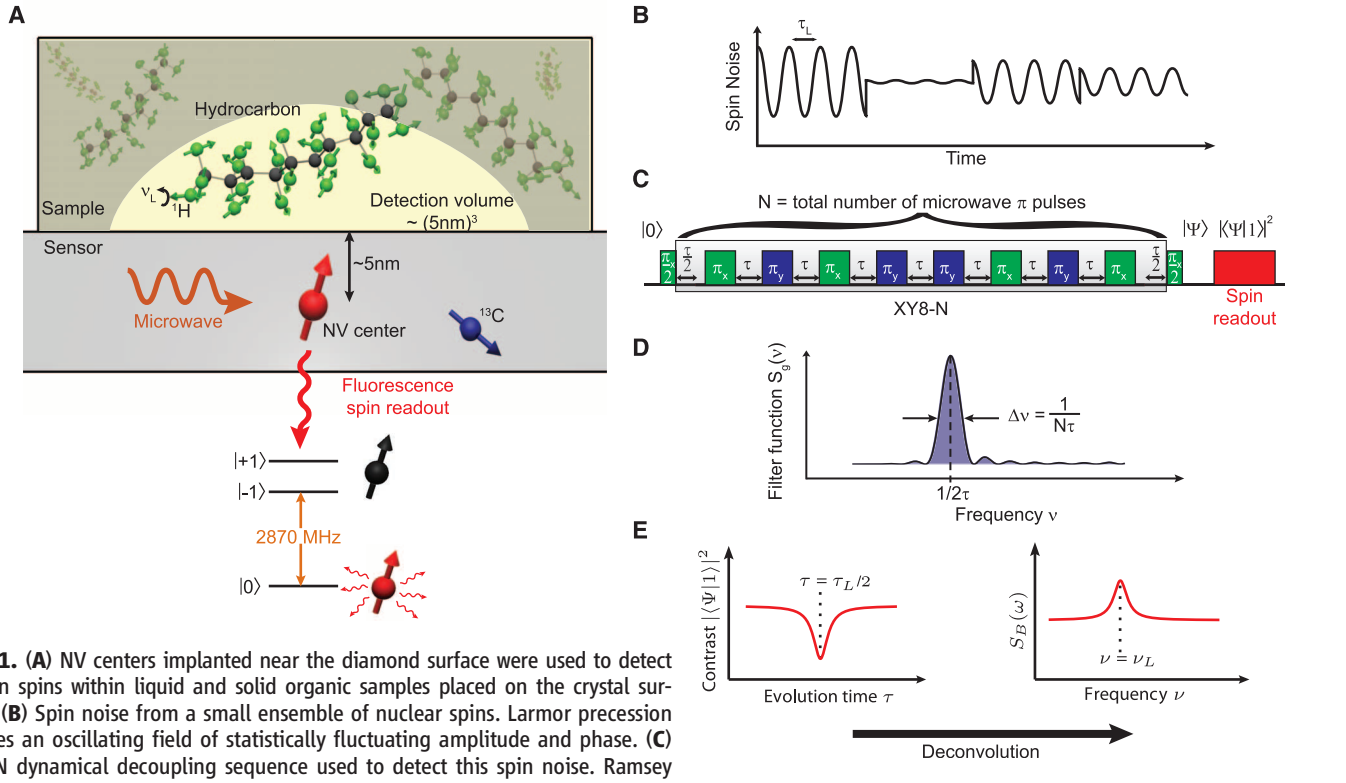

Fig. 1. (**A**) NV centers implanted near the diamond surface were used to detect proton spins within liquid and solid organic samples placed on the crystal surface. (**B**) Spin noise from a small ensemble of nuclear spins. Larmor precession creates an oscillating field of statistically fluctuating amplitude and phase. (**C**) XY8-N dynamical decoupling sequence used to detect this spin noise. Ramsey interferometry by an initial and final $\pi/2$ pulse measures the magnetic field. A train of N π pulses acts as a filter to select a specific frequency component of the noise. (**D**) Filter function of the pulse sequence, peaking at one specific frequency $1/2\tau$. (**E**) Repeating the sequence for varying pulse spacing τ yields a spectrum of the spin noise.

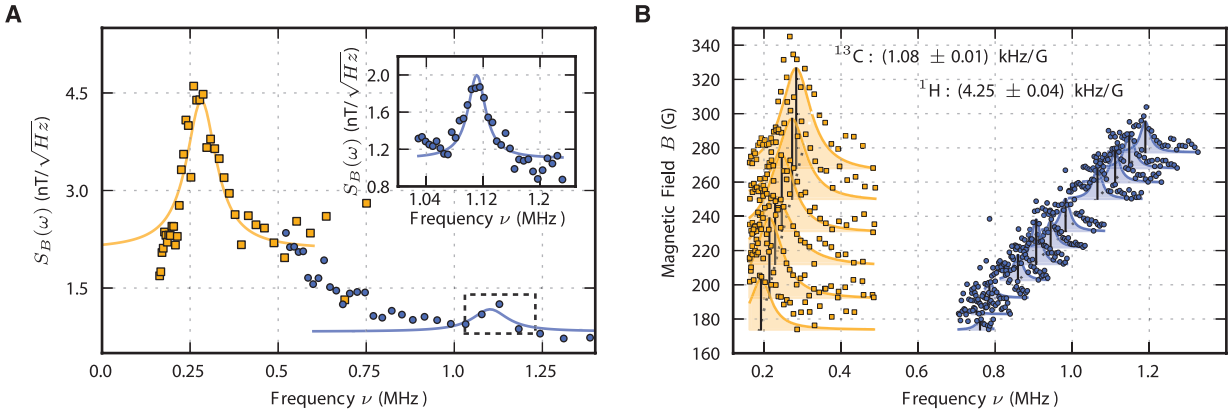

Fig. 2. (**A**) NMR spectrum of statistically polarized nuclei in the vicinity of a shallow implanted NV center. A strong contribution of ^{13}C nuclei inside the diamond [yellow, acquired by a CPMG6 sequence (*20*)] was accompanied by a weaker component of ^{1}H nuclei of the sample (blue, acquired using a XY8-160 sequence and a sample of microscopy immersion oil). (**B**) Both components shifted with the magnetic field at the gyromagnetic ratios of the respective species.

10 nm below the surface of the diamond by ion implantation (*16*) with a sample of organic material placed on the diamond surface [see supplementary material (*17*)].

Our technique for detecting the magnetic field of protons in the sample is based on measuring the statistical polarization of the spin population near the NV center with a dynamical decoupling method (Fig. 1, B to E). The magnetic field at the NV center is dominated by a small number of nearest protons (on the order of 10^4). The net magnetization of this small set of randomly oriented spins is zero but has a sizable standard deviation equivalent to $\sqrt{N} = 10^2$ protons. Equivalently, this excess amount of protons can be considered to be statistically polarized along a random direction (*18*, *19*). In particular, this statistical polarization will lead to a random magnetization $\langle M_x\rangle$,$\langle M_y\rangle$ in the transverse plane, which undergoes Larmor precession under the applied magnetic field and leads to an oscillating field component $B_z = B(\langle M_x\rangle, \langle M_y\rangle)\cos(2\pi t/\tau_{\mathrm{Larmor}} + \phi)$ along the axis of the NV center.

We detected this oscillating component using dynamical decoupling ac magnetometry based on the XY8-N pulse sequence (*20*–*26*) (Fig. 1C). Here, an initial $\pi/2$ microwave pulse places the NV center into a coherent superposition $(|0\rangle + e^{i\phi}|1\rangle)/\sqrt{2}$ of two spin states. Its phase ϕ is sensitive to the fluctuating magnetic field and evolves from $\phi = 0$ at the beginning of the sequence to a nonzero random phase $\phi = \Delta\phi$, which is converted into a population difference of the states by a final $\pi/2$ pulse and subsequently read out. For a fluctuating magnetic field, this phase is a random variable with variance $\langle\Delta\phi^2\rangle$, which, when averaged over many repetitions, reduces the readout contrast obtained after the final $\pi/2$ pulse to

$$C = 2|\langle 1|\psi\rangle|^2 - 1 = e^{-\langle\Delta\phi^2\rangle/2}$$

The phase $\langle\Delta\phi^2\rangle$ is made sensitive to specific frequency components by periodically flipping the NV spin by a train of N equidistant π pulses between the initial and final $\pi/2$ pulse. This "quantum lock-in detection" (*23*) enhances sensitivity to all fields oscillating synchronously with the pulse spacing τ, while it suppresses the effect of field fluctuations at every other frequency. More precisely

$$\langle\Delta\phi^2\rangle = \gamma^2 \sum_{n=-\infty}^{\infty} S_g(\nu_n) S_B(\nu_n)$$

where $\gamma = g\mu_B/\hbar$ is the NV spin's gyromagnetic ratio, $\nu_n = n/N\tau$, $S_B(\nu_n)$ is the power spectral density of magnetic field fluctuations, and the filter function $S_g(\nu_n)$ is a function sharply peaked around the frequency $1/2\tau$ encoding the effect of the π-pulse train (Fig. 1D). Repeating the experiment for varying pulse spacings τ, we can sample the entire spectrum $S_B(\nu_n)$ and hence record a NMR spectrum of statistically polarized nuclei in the vicinity of the center.

A typical spectrum obtained from such an experiment (Fig. 2A) is dominated by a strong peak at the ^{13}C Larmor frequency, corresponding to spin noise from intrinsic nuclei of the diamond lattice. Under high-order dynamical decoupling, sensitivity increased sufficiently to reveal an additional smaller peak (blue line in Fig. 2A) that we attribute to protons from the sample placed on the diamond surface. Its frequency scales linearly with magnetic field (Fig. 2B) with a slope of 4.25 ± 0.04 kHz/G, the gyromagnetic ratio of ^{1}H.

We could reversibly switch the signal seen by a given NV center by coating the surface with different solid and liquid compounds (Fig. 3A). The signal was visible under a coating of immersion oil (yellow circles), but it completely vanished under a coating of a deuterated polymer (^{2}H-PMMA, blue triangles) and subsequently reappeared when the surface was coated with its natural-abundance equivalent (green squares). We also demonstrated basic spectroscopy by recording several high-resolution spectra (Fig. 3B). Under a PMMA coating, we measured a broadened linewidth of 46.3 ± 1.5 kHz (obtained from a Lorentzian fit), which agrees well with reported data (*27*). Spectroscopy under a

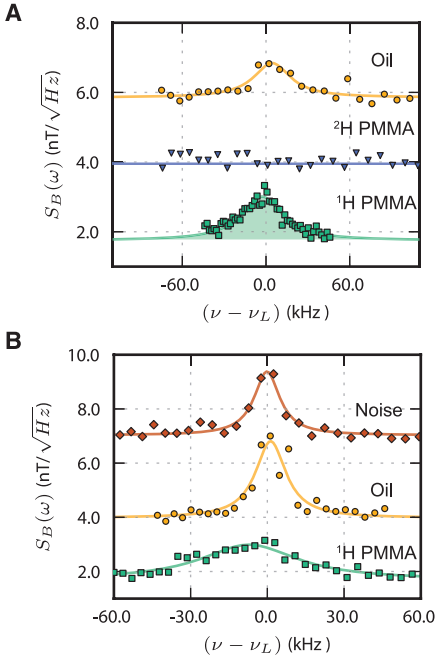

Fig. 3. (**A**) NMR spectra obtained successively on the same center with an XY8-80 sequence under coatings of a liquid sample (immersion oil, yellow points), a deuterated solid (^{2}H PMMA, blue triangles), and a protonated solid sample (^{1}H PMMA, green squares). (**B**) High-resolution spectra (XY8-112). Green squares: Spectrum under a polymer coating (^{1}H PMMA). Yellow circles: Spectrum under immersion oil, obtained on the same NV. Tilted red squares: Spectral resolution of our scheme, obtained on a different NV by applying externally generated magnetic field noise of fixed frequency. Spectra are offset along the *y* axis to enhance readability.

liquid sample reveals a narrow line (oil, Fig. 3B), as expected from rotational narrowing. Its linewidth of 14.4 ± 0.4 kHz was still four orders of magnitude greater than typical values for bulk liquid NMR, which can be explained by two effects. First, diffusion through the nanoscale sample volume can randomize polarization on a fast

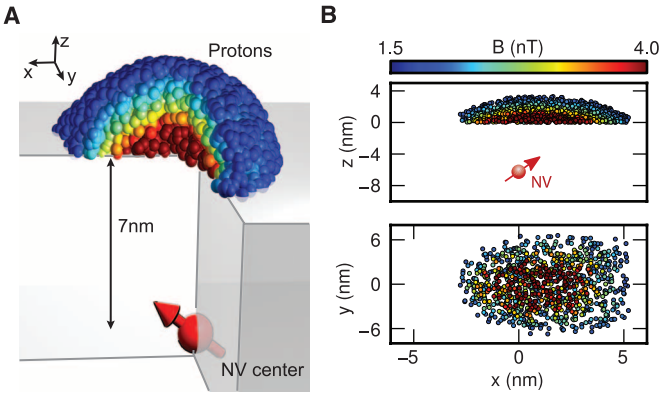

Fig. 4. Numerical simulation of the detection volume. **(A)** Three-dimensional visualization of the 10^4 closest protons (spheres), generating 70% of the signal. Protons are color-coded by their contribution to the total signal. **(B)** Two-dimensional projections of (A).

time scale and broaden the line. Second, the line was substantially broadened by our spectral resolution (12.2 ± 0.3 kHz, upper curve of Fig. 3B). This experimental resolution could be improved by increasing N, the order of dynamical decoupling, which should allow for an ultimate resolution of $\Delta\nu/\nu \approx (T_{1,NV}\Omega_{R,NV})^{-1} \approx 1$ppm, with $T_{1,NV}\Omega_{R,NV}$ denoting the relaxation time and Rabi frequency of the NV, respectively (*28*, *29*).

The integrated, background-corrected field strength experienced under a coating of PMMA by a typical NV center is $B_{rms} = 390 \pm 60$ nT (green shaded area in Fig. 3A). According to an analytical model of the proton magnetic field (*30*), assuming a homogeneous proton density of 5×10^{28} m^{-3}, this field strength corresponds to an NV center located 6.4 ± 0.7 nm below the surface. Numerical simulations of the ion implantation predict a similar value (*17*). This suggests that our result can yield a nondestructive method to measure the depth of an individual center with nanometer statistical uncertainty.

We confirmed the signal magnitude by a numerical simulation, which explicitly computes the field of 4×10^5 protons, placed at random locations in a cube of 20-nm width. We found that 70% of the signal was generated by the 10^4 closest protons, corresponding to a detection volume of only (5 nm)^3 (Fig. 4), which is comparable to that of a medium-size (100-kD) protein.

An important extension of our results will be the combination with scanning NV centers (*14*, *15*) to implement NMR imaging at the nanoscale. Being based on statistical rather than thermal polarization, our approach enables the acquisition of NMR spectra of an arbitrary substance at low magnetic fields, down to and including zero field, without the need for prepolarization (*31*). In this regime, magic angle spinning can be realized by rotating the external field rather than the sample. This allows for higher rotation frequencies than at high field, which is potentially of great benefit for solid-state NMR. Finally, we anticipate that our technique can yield a new method of hyperpolarization for arbitrary samples by coherently transferring the polarization of the NV spin to the sample. We estimate that full polarization of the detection volume might be achievable. The transfer of one quantum of angular momentum would occur on the time scale of our detection (~20 μs), and hence 10^4 transfers can be completed on a time scale faster than the protons' longitudinal relaxation time T_1 (typically on the order of seconds).

References and Notes

1. F. Bloch, *Phys. Rev.* **70**, 460 (1946).
2. E. M. Purcell, H. C. Torrey, R. V. Pound, *Phys. Rev.* **69**, 37 (1946).
3. D. Rugar, R. Budakian, H. J. Mamin, B. W. Chui, *Nature* **430**, 329 (2004).
4. C. L. Degen, M. Poggio, H. J. Mamin, C. T. Rettner, D. Rugar, *Proc. Natl. Acad. Sci. U.S.A.* **106**, 1313 (2009).
5. L. Ciobanu, D. A. Seeber, C. H. Pennington, *J. Magn. Reson.* **158**, 178 (2002).
6. A. Blank, J. H. Freed, *Isr. J. Chem.* **46**, 423 (2007).
7. A. Gruber *et al.*, *Science* **276**, 2012 (1997).
8. F. Jelezko, T. Gaebel, I. Popa, A. Gruber, J. Wrachtrup, *Phys. Rev. Lett.* **92**, 076401 (2004).
9. J. M. Taylor *et al.*, *Nat. Phys.* **4**, 810 (2008).
10. G. Balasubramanian *et al.*, *Nat. Mater.* **8**, 383 (2009).
11. T. H. Taminiau *et al.*, *Phys. Rev. Lett.* **109**, 137602 (2012).
12. S. Kolkowitz, Q. P. Unterreithmeier, S. D. Bennett, M. D. Lukin, *Phys. Rev. Lett.* **109**, 137601 (2012).
13. N. Zhao *et al.*, *Nat. Nanotechnol.* **7**, 657 (2012).
14. G. Balasubramanian *et al.*, *Nature* **455**, 648 (2008).
15. P. Maletinsky *et al.*, *Nat. Nanotechnol.* **7**, 320 (2012).
16. J. Meijer *et al.*, *Appl. Phys. Lett.* **87**, 261909 (2005).
17. Supplementary materials are available on *Science* Online.
18. C. L. Degen, M. Poggio, H. J. Mamin, D. Rugar, *Phys. Rev. Lett.* **99**, 250601 (2007).
19. F. Reinhard *et al.*, *Phys. Rev. Lett.* **108**, 200402 (2012).
20. L. Cywiński, R. M. Lutchyn, C. P. Nave, S. Das Sarma, *Phys. Rev. B* **77**, 174509 (2008).
21. G. de Lange, D. Ristè, V. V. Dobrovitski, R. Hanson, *Phys. Rev. Lett.* **106**, 080802 (2011).
22. A. Laraoui, J. S. Hodges, C. A. Meriles, *Appl. Phys. Lett.* **97**, 143104 (2010).
23. S. Kotler, N. Akerman, Y. Glickman, A. Keselman, R. Ozeri, *Nature* **473**, 61 (2011).
24. J. Bylander *et al.*, *Nat. Phys.* **7**, 565 (2011).
25. L. T. Hall, J. H. Cole, C. D. Hill, L. C. L. Hollenberg, *Phys. Rev. Lett.* **103**, 220802 (2009).
26. N. Bar-Gill *et al.*, *Nat. Commun.* **3**, 858 (2012).
27. K. M. Sinnott, *J. Polym. Sci., Polym. Phys. Ed.* **42**, 3 (1960).
28. E. C. Reynhardt, G. L. High, J. A. van Wyk, *J. Chem. Phys.* **109**, 8471 (1998).
29. G. D. Fuchs, V. V. Dobrovitski, D. M. Toyli, F. J. Heremans, D. D. Awschalom, *Science* **326**, 1520 (2009).
30. C. A. Meriles *et al.*, *J. Chem. Phys.* **133**, 124105 (2010).
31. M. P. Ledbetter *et al.*, *Proc. Natl. Acad. Sci. U.S.A.* **105**, 2286 (2008).

Acknowledgments: We thank L. Häussler, D. Antonov, A. Denisenko, and A. Aird for sharing cTRIM and molecular dynamics simulation data and G. Majer and T. Bräuninger for bulk NMR measurements, as well as H. J. Mamin, D. Rugar, and P.-G. Reinhard for helpful discussions. This work was supported by the European Union (SQUTEC, DIAMANT), the Max Planck Society, Deutsche Forschungsgemeinschaft (SFB/TR21, Research groups 1493 and 1482, SPP1601), Defense Advanced Research Projects Agency (QUASAR program), Volkswagen Foundation, contract research of the Baden-Württemberg foundation ("Methoden für die Lebenswissenschaften"), the 973 Program (2013CB921800), NNSFC (11227901, 91021005, 10834005), and Chinese Academy of Sciences. T.S. acknowledges financial support from the IMPRS-AM and C.A.M. from the Humboldt Foundation and the NSF (NSF-1111410).

Supplementary Materials

www.sciencemag.org/cgi/content/full/339/6119/561/DC1
Materials and Methods
Supplementary Text
Figs. S1 to S7
References (*32*, *33*)

17 October 2012; accepted 3 December 2012
10.1126/science.1231675

Detecting Ozone- and Greenhouse Gas–Driven Wind Trends with Observational Data

Sukyoung Lee[1]* and Steven B. Feldstein[1]

Modeling studies suggest that Antarctic ozone depletion and, to a lesser degree, greenhouse gas (GHG) increase have caused the observed poleward shift in the westerly jet during the austral summer. Similar studies have not been performed previously with observational data because of difficulties in separating the two contributions. By applying a cluster analysis to daily ERA-Interim data, we found two 7- to 11-day wind clusters, one resembling the models' responses to GHG forcing and the other resembling ozone depletion. The trends in the clusters' frequency of occurrence indicate that the ozone contributed about 50% more than GHG toward the jet shift, supporting the modeling results. Moreover, tropical convection apparently plays an important role for the GHG-driven trend.

Throughout the late 20th century, the Southern Hemisphere (SH) westerlies have undergone a poleward shift (*1*–*3*), especially during the austral summer (December through February; DJF hereafter) (Fig. 1A). This change affects weather and climate not only by altering the